ACS Macro Letters

Letter

pubs.acs.org/macroletters

# 3D Printing Phosphonium Ionic Liquid Networks with Mask Projection Microstereolithography

Alison R. Schultz,[‡] Philip M. Lambert,[†] Nicholas A. Chartrain,[†] David M. Ruohoniemi,[‡] Zhiyang Zhang,[‡] Chainika Jangu,[‡] Musan Zhang,[‡] Christopher B. Williams,[†] and Timothy E. Long*[,‡]

[†]Department of Mechanical Engineering and [‡]Macromolecular and Interfaces Institute, Department of Chemistry, Virginia Tech, Blacksburg, Virginia 24061, United States

Supporting Information

**ABSTRACT:** Photopolymerization coupled with mask projection microstereolithography successfully generated various 3D printed phosphonium polymerized ionic liquids (PILs) with low UV light intensity requirements and high digital resolution. Varying phosphonium monomer concentration, diacrylate cross-linking comonomer, and display images enabled precise 3D design and polymeric properties. The resulting cross-linked phosphonium PIL objects exhibited a synergy of high thermal stability, tunable glass transition temperature, optical clarity, and ion conductivity, which are collectively well-suited for emerging electro-active membrane technologies. Ion conductivity measurements on printed objects revealed a systematic progression in conductivity with ionic liquid monomer content, and thermal properties and solvent extraction demonstrated the formation of a polymerized ionic liquid network, with gel fractions exceeding 95%.

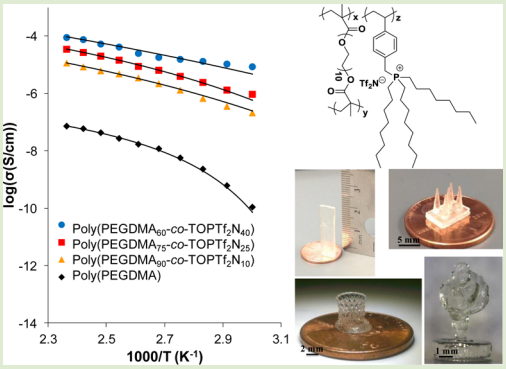


Ionic liquid monomers provide unique macromolecules that incorporate cationic sites either pendant to or within the polymer backbone with an accompanying mobile counteranion. These charged polymers provide beneficial properties such as a complement of ionic conductivity, thermal and chemical stability, and anion exchange capability. Most studies describe polymers containing ammonium, imidazolium, and 1,2,3-triazolium cations with mobile counteranions such as halides, tetrafluoroborate ($BF_4$), hexafluorophosphate ($PF_6$), and bis(trifluoromethanesulfonyl)imide ($Tf_2N$).[1−3] Our current research has demonstrated advantages of phosphonium polymerized ionic liquids (PILs) with improved thermal stability, enhanced ion conductivity, and more efficient nucleic acid delivery compared to ammonium and imidazolium analogues. Limited commercial availability of phosphonium monomers impeded the design of phosphonium PILs and favored the development of ammonium and imidazolium PIL derivatives. However, an expanded commercial phosphine library has recently enabled the synthesis of low viscosity, high conductivity phosphonium monomers, and resulted in the production of diverse phosphonium-containing macromolecules, including homopolymers,[4] random copolymers,[5] and block copolymers.[6] Current research efforts reveal phosphonium PILs as candidates for ion conducting membranes due to the cationic functionality within each polymeric repeat unit, and the earlier literature suggests impact on technologies ranging from electromechanical actuators[7−9] and gas separation membranes[10−12] to ion exchange membranes.[13−17] The simultaneous enhancement in thermal stability and ion conductivity for phosphonium PILs promises opportunities to enable higher temperature applications, which is critical for demanding aerospace, electronics, and transportation industries.

Enhanced thermal stability of phosphonium PILs stems from a preferred degradation process involving a high temperature nucleophilic substitution mechanism, unlike ammonium derivatives that generally favor Hofmann elimination with a counteranion abstraction of a $\beta$-hydrogen. Long et al. recently described these mechanisms in a systematic comparison between ammonium and phosphonium PILs, which examined structure−property relationships and elucidated the influence of cation selection, alkyl substituent length, and counteranion on thermal properties, ionic conductivities, and morphologies.[18] Elabd and Winey et al. also extensively examined structure−property relationships of imidazolium PILs and reported the impact of counteranion selection and functional substituents on tailoring PIL glass transition temperature ($T_g$) and electrochemical properties for enhancing ionic conductivity.[19] These studies systematically confirmed that reduced $T_g$ values favored increased ionic conductivity. Other precedent literature supports these claims and specifically describes trifluoromethanesulfonate (TfO) and bis(trifluoromethanesulfonate)imide ($Tf_2N$) counteranions to tune $T_g$ and ionic conductivity.[20,21] Various polymerization and postpolymerization strategies for synthesizing phosphonium PILs exist in the literature. McGrath et al. reported the synthesis of poly(arylene ether) main chain

**Received:** October 3, 2014
**Accepted:** November 3, 2014
**Published:** November 6, 2014

  

phosphonium-containing ionomers for high-performance applications, such as ion exchange membranes.[22] Long et al. studied structure−property relationships of random and block copolymers involving phosphonium styrenic salts containing either methyl, ethyl, propyl, butyl, or octyl chains.[5,6,18,23] Other synthetic studies disclose atom transfer (ATRP)[24] and reversible addition−fragmentation transfer (RAFT)[25,26] polymerization methods for achieving well-defined phosphonium PILs.

Concurrent advances in fabricating devices from novel monomers and polymers are also needed to meet these technologies. Additive manufacturing, often referred to as 3D printing, where objects are constructed in a layer-by-layer fashion, enables the design and creation of geometrically complex objects with tailored topology, and thus, functionality. Stereolithography (SL), a well-established additive manufacturing technology, is used to create objects with features <100 $\mu$m by selectively scanning an ultraviolet (UV) laser beam across a reservoir of photopolymer resin. In mask projection microstereolithography (MP$\mu$SL), a modification of the SL process, an entire cross-sectional layer of photopolymer is cured upon projecting digitally patterned UV light with a dynamic mask (e.g., a digital micromirror device, commonly found in digital projectors).[27] Unlike traditional SL processes, the laser beam radius or scan speed does not limit MP$\mu$SL and, thus, enables the fabrication of feature sizes smaller than 10 $\mu$m, while also reducing build times by an order-of-magnitude.[28−30] MP$\mu$SL's ability to selectively pattern UV light in a layer-by-layer fabrication process provides the opportunity for tailoring polymer architecture and material properties across multiple length scales in 3D space. The goal of this work is therefore to develop photo-cross-linkable ionic liquids for this process to enable the production of complex micron-scale electromechanical objects. Herein, we report photopolymerization strategies coupled with additive manufacturing to achieve 3D printed phosphonium PILs in order to demonstrate the first example of 3D printing of an ion-conducting polymer. Conventional strategies for printing ion-conducting materials are limited to conductive composites, which require additional production cost and energy, and often results in printed objects with potential composite leaching. We introduce the potential synergy between MP$\mu$SL technology and ionic liquids to form cross-linked networks with chemically bound charged species for enhanced charge stability and extended ion-conductivity.

Scheme 1A depicts the synthetic strategy for achieving the phosphonium ionic liquid monomer, 4-vinylbenzyl trioctyl phosphonium bis(trifluoromethanesulfonate)imide ($TOPTf_2N$). Subsequent quantitative anion exchange of the phosphonium chloride salt precursor (TOPCl) with $Tf_2N$ resulted in the $TOPTf_2N$ liquid monomer at room temperature, which exhibited a melting temperature ($T_m$) below −90 °C and an onset of degradation temperature ($T_d$) of 420 °C. The notably low $T_m$ for $TOPTf_2N$ classifies the monomer as a polymerizable room temperature ionic liquid, while the high $T_d$ value suggests the potential for poly($TOPTf_2N$) in high-temperature electro-active devices. The anion exchanged monomer did not dissolve in nonpolar solvents such as hexanes in contrast to the precursor TOPCl. This counteranion dependent solubility suggested that the association between the phosphonium cation and the bulky $Tf_2N$ anion was relatively weak.

$TOPTf_2N$ unexpectedly revealed improved miscibility with polar reagents, including UV-curable diacrylic monomers such as 1,4-butanediol diacrylate (BDA) and poly(ethylene glycol) dimethacrylate (PEGDMA). This enabled diverse photocured poly(BDA-*co*-$TOPTf_2N$) and poly(PEGDMA-*co*-$TOPTf_2N$) cross-linked networks with increasing mol % incorporation of $TOPTf_2N$ phosphonium ionic liquid monomer. UV-curing $TOPTf_2N$ ionic liquid monomer into traditional poly(BDA) and poly(PEGDMA) cross-linked networks offers an opportunity to impart thermally stable charged sites for improving ion mobility, gas diffusion, and salt permeability. Tuning these properties with phosphonium ionic liquid concentration will tailor resulting electro-active membranes for advanced applications in batteries,[31,32] gas separation,[33,34] and water desalination.[35,36]

Scheme 1B depicts the photopolymerization of poly(BDA-*co*-$TOPTf_2N$) and poly(PEGDMA-*co*-$TOPTf_2N$) cross-linked networks, including 2 wt % of the photoinitiator 2,2-dimethoxy-1, 2-diphenylethan-1-one and exposure to a 365 nm UV light source. Photorheology investigations evaluated the effects of UV light intensity on cure time and storage modulus ($G'$) of the cross-linked networks, which enabled a comparison in structure-processing relationships between poly(PEGDMA), poly(BDA), poly($PEGDMA_{90}$-*co*-$TOPTf_2N_{10}$), and poly($BDA_{90}$-*co*-$TOPTf_2N_{10}$) networks (Figure 1). Increasing UV

**Scheme 1. (A) Anion Exchange of Phosphonium 4-Vinylbenzyl Trioctyl Phosphonium Chloride; (B) Synthesis of Poly(PEGDMA-*co*-$TOPTf_2N$) and Poly(BDA-*co*-$TOPTf_2N$) Crosslinked 3D Networks**

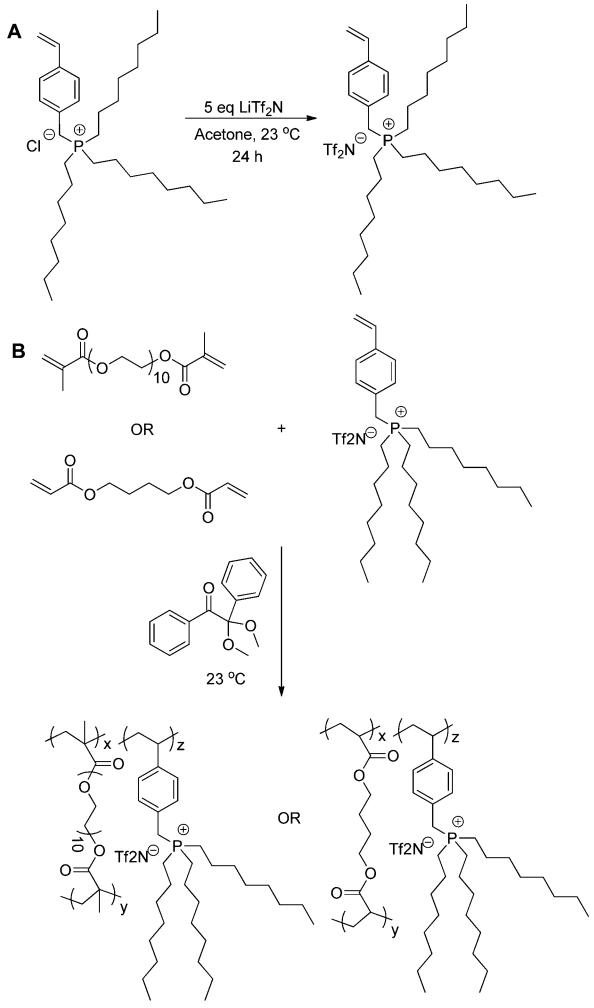



dx.doi.org/10.1021/mz5006316 | ACS Macro Lett. 2014, 3, 1205−1209

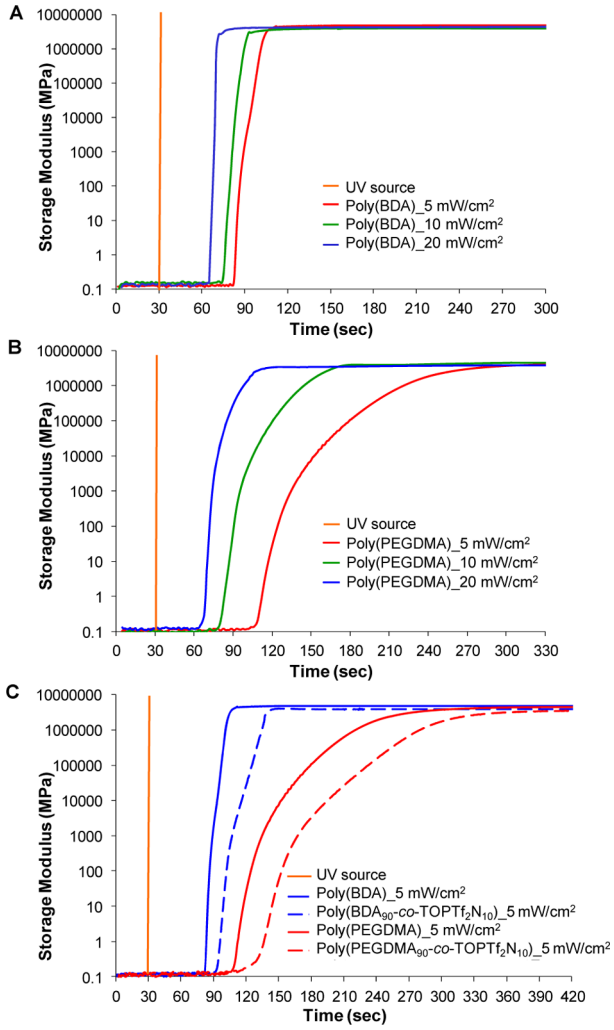


**Figure 1.** Photorheology characterization of (A) poly(BDA) and (B) poly(PEGDMA) at various light intensity exposure. (C) Photorheology characterization comparing structure-processing relationships between poly(BDA), poly(PEGDMA), poly(BDA$_{90}$-*co*-TOPTf$_2$N$_{10}$), and poly(PEGDMA$_{90}$-*co*-TOPTf$_2$N$_{10}$) at 5 mW/cm$^2$ light intensity exposure.

light intensity of 5, 10, and 20 mW/cm$^2$ revealed faster cure times for all samples while maintaining a two step $G'$ transition, corresponding to the approximate gel point transition from a viscous to solid state during photopolymerization. Overlaying the photorheology data for the cross-linked networks at 5 mW/cm$^2$ elucidated the photoprocessing differences between PEGDMA- and BDA-containing networks, revealing slower cross-linking of PEGDMA chains in comparison to the BDA monomer. The extended photocuring time correlated to the ethylene oxide spacer within the PEGDMA cross-linking agent, which also advantageously reduces the $T_g$ and imparts network flexibility during photocuring at room temperature.

Photopolymerization strategies for UV-curing poly(PEGDMA-*co*-TOPTf$_2$N) cross-linked networks coupled with MP$\mu$SL technology achieved layer-by-layer fabrication of poly(PEGDMA-*co*-TOPTf$_2$N) cross-linked 3D objects. Literature reports thoroughly detail the MP$\mu$SL operating system apparatus.[27] The process involves a light emitting diode (LED) that projects light into a series of conditioning optics, which includes collimating lenses, wavelength filters, and homogenizing rods. A mirror reflects the conditioned light onto a dynamic pattern generator (dynamic mask) parallel to the projection surface, which then digitally patterns and projects the incident light as an image. Finally, an optical lens resizes the patterned light in order to focus the final image on the surface of photocurable viscous monomers or oligomers. The projected pattern initiates the cross-linking of monomer or oligomers, causing a change in phases from a liquid to a solid state during photopolymerization. During a layer-by-layer process, the first layer of photocurable monomer or oligomer is cured on a build platform under an UV intensity of 4.9 mW/cm$^2$ (Figure S1). The build platform repositions such that additional viscous monomer or oligomer recoats the previously cured polymer to provide material for creating a subsequent layer. An image of the next cross-sectional layer projects onto the subsequent layer and the photocuring process repeats until achieving a final 3D object.

A diverse range of computer-aided design (CAD) files enable the additive manufacturing of diverse 3D printed poly(PEGDMA-*co*-TOPTf$_2$N) objects, ranging from 33 mm tall rectangular test specimens to 8 mm tall 3D cones, hyperboloids, and figurines (Figure 2). X-ray microCT scanning

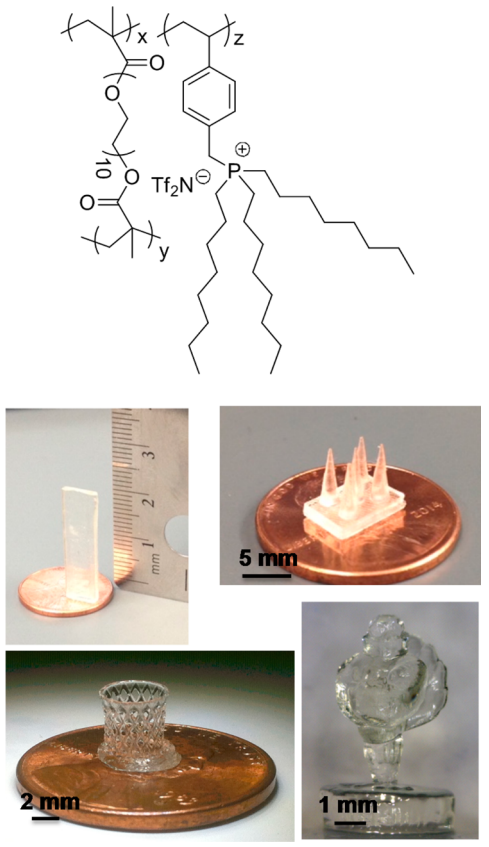


**Figure 2.** Mask projection microstereolithography successfully 3D prints poly(PEGDMA-*co*-TOPTf$_2$N) 33 mm tall rectangular test specimens, 8 mm tall cones, 8 mm tall hyperboloid, and 8 mm tall figurine.

reconstructed a CAD image of the poly(PEGDMA$_{90}$-*co*-TOPTf$_2$N$_{10}$) 3D cones, demonstrating systematic efficiency in reproducing CAD designs (Figure 3). Scanning electron microscopy (SEM) images of the poly(PEGDMA$_{90}$-*co*-TOPTf$_2$N$_{10}$) 3D hyperboloid depicts well-defined architecture and build reproducibility in the complex object (Figure 4). The surface roughness depicted in both X-ray microCT and SEM


dx.doi.org/10.1021/mz5006316 | *ACS Macro Lett.* 2014, 3, 1205−1209

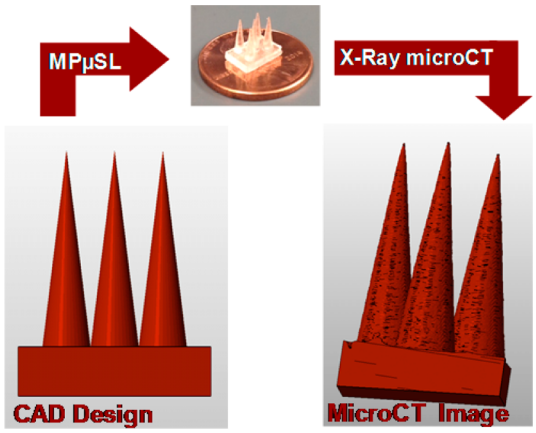


**Figure 3.** X-ray microCT image of 3D printed poly(PEGDMA90-*co*-$TOPTf_2N_{10}$) cones in comparison to original CAD design.

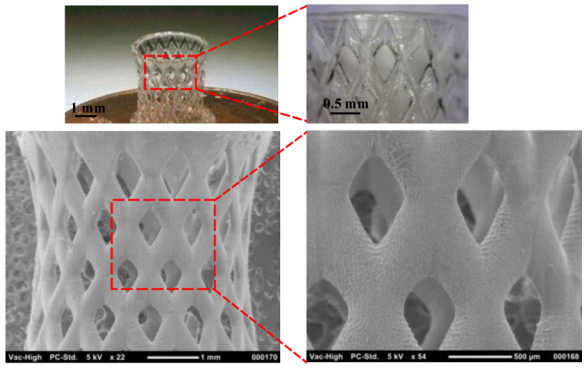


**Figure 4.** Detailed images of 3D printed poly(PEGDMA90-*co*-$TOPTf_2N_{10}$) hyperboloid with optical microscopy and scattering electron microscopy.

images is consistent for all printed objects and is attributed to the microstereolithography build process.

Varying the mol % incorporation of $TOPTf_2N$ achieved a series of 3D, 33 mm × 6 mm × 2 mm test specimens including poly(PEGDMA), poly($PEGDMA_{95}$-*co*-$TOPTf_2N_5$), poly($PEGDMA_{90}$-*co*-$TOPTf_2N_{10}$), poly($PEGDMA_{75}$-*co*-$TOPTf_2N_{25}$), and poly($PEGDMA_{60}$-*co*-$TOPTf_2N_{40}$). Soxhlet extraction with THF at reflux for 24 h determined wt % gel fraction for all test specimens, revealing gel fractions of 93−97 wt % and confirming high UV-curing efficiency (Table 1). Thermogravimetric analysis (TGA) probed the thermal properties for the various poly(PEGDMA-*co*-$TOPTf_2N$) samples and confirmed corresponding target wt % incorporation of $TOPTf_2N$ (Table 1 and Figure S2). The TGA transitions for the poly(PEGDMA-*co*-$TOPTf_2N$) samples exhibited a two-step thermal degradation profile with the initial step ($T_{d,5\%wtloss}$) occurring at approximately 320 °C, corresponding to PEGDMA degradation, and the second step occurring at approximately 420 °C, correlating with the $T_d$ of $TOPTf_2N$. Increasing mol % incorporation of $TOPTf_2N$ resulted in two-step weight loss profiles that varied in wt % remaining. For poly(PEGDMA-*co*-$TOPTf_2N$) test specimens with 5, 10, 25, and 40 mol % $TOPTf_2N$, second step TGA transitions revealed an increase in wt % remaining values that corresponded to 7, 13, 30, and 46 wt % $TOPTf_2N$. The observed increase in wt % $TOPTf_2N$ compared well to the mol % values and confirmed the incorporation of the $TOPTf_2N$. Differential scanning calorimetry (DSC) elucidated the effects of increasing $TOPTf_2N$ content on $T_g$ values for the 3D fabricated poly(PEGDMA-*co*-$TOPTf_2N$) test specimens (Table 1). As anticipated for cross-linked networks, increasing mol % content of $TOPTf_2N$ resulted in an observable slight depression in $T_g$. The control poly(PEGDMA) sample revealed a $T_g$ of −10 °C, which gradually decreased to −18 °C for 40 mol % $TOPTf_2N$. The observed trend in decreasing $T_g$ correlated to the increasing content of polymerized phosphonium ionic liquid within the photo-cross-linked PEGDMA matrix.

Consistent with previous literature reports, a lower $T_g$ increased ionic conductivity for the 3D fabricated poly(PEGDMA-*co*-$TOPTf_2N$) test specimens (Figure 5). Ionic

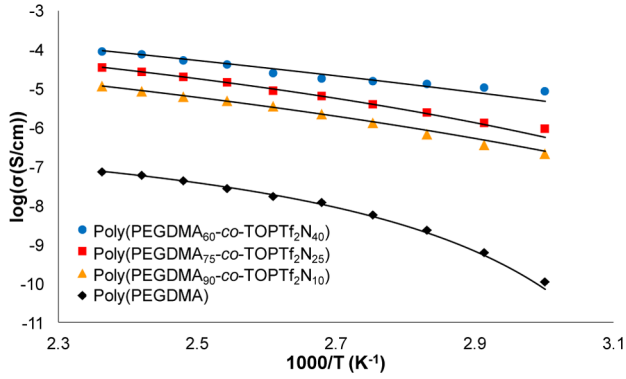


**Figure 5.** Ionic conductivity for poly(PEGDMA-*co*-$TOPTf_2N$) 3D printed rectangular films with 10, 25, and 40 mol % $TOPTf_2N$. The relative humidity was maintained at 10% over the 60 to 150 °C.

conductivity in single-ion conductors strongly depends on frequency and temperature.[37] The value of DC conductivity is defined as the in-phase component of the conductivity, which is independent of frequency over a 3-decade frequency range. Poly($PEGDMA_{60}$-*co*-$TOPTf_2N_{40}$), which has the highest mol % of the phosphonium ion-conducting units, exhibited the highest ionic conductivity and the lowest $T_g$. Ionic conductivity decreased with increasing mol % of PEGDMA and correlated

**Table 1. Thermal Properties, Percent Gel Fraction, and VFT Fitting and Analysis of PIL Conductivity Data for Poly(PEGDMA-*co*-$TOPTf_2N$) 3D Printed Rectangular Test Specimens**[a]

| sample | % gel fraction | $T_{d,1}$ (°C) | $T_{d,1}$ (wt%) | $T_{d,2}$ (°C) | $T_{d,2}$ (wt%) | $T_g$ (°C) | $\sigma_{inf}$ (S·cm$^{-1}$) | $B$ (K) | $T_0$ (K) |
|---|---|---|---|---|---|---|---|---|---|
| cross-linked PEGDMA | 94 | 320 | 100 | NA | NA | −10 | −5.75 | 411 | 292 |
| poly($PEGDMA_{95}$-*co*-$TOPTf_2N_5$) | 95 | 320 | 91 | 420 | 9 | −10 | NA | NA | NA |
| poly($PEGDMA_{90}$-*co*-$TOPTf_2N_{10}$) | 97 | 320 | 83 | 420 | 15 | −14 | −2.34 | 1376 | 193 |
| poly($PEGDMA_{75}$-*co*-$TOPTf_2N_{25}$) | 95 | 330 | 68 | 420 | 35 | −16 | −2.15 | 1085 | 217 |
| poly($PEGDMA_{60}$-*co*-$TOPTf_2N_{40}$) | 93 | 330 | 60 | 420 | 40 | −18 | −1.04 | 2034 | 127 |

[a]% gel fraction: wt% remaining after reflux in THF for 24 h; $T_{d,1}$: first step thermal degradation; $T_{d,2}$: second step thermal degradation.


dx.doi.org/10.1021/mz5006316 | ACS Macro Lett. 2014, 3, 1205−1209

closely with the phosphonium-containing charge concentration, where the poly(PEGDMA) revealed the lowest ionic conductivity. These results agreed with our previous studies that compared conductivity of phosphonium and ammonium PILs, revealing a comparable conductivity range at the operating temperature for the cross-linked networks with increasing phosphonium PIL content. All specimens for conductivity measurements were performed at 10% relative humidity, and the control poly(PEGDMA) agreed with earlier reports.[38] While the effects of a lowered $T_g$ optimized ionic conductivity, TGA-sorption analysis also confirmed negligible effects of water adsorption of poly(PEGDMA-*co*-TOPTf$_2$N) test specimens. While increasing mol % of TOPTf$_2$N revealed increasing water uptake with time, the hydrophobic Tf$_2$N counteranion in a PEGDMA matrix limited water uptake to less than 0.5 wt %.

Future studies will focus on expanding phosphonium PILs into more complex and well-defined conductive objects for emerging electro-active membrane technologies. Varying phosphonium charge concentration, cross-linking monomers, and digital images will enable the construction of diverse 3D printed phosphonium PILs with tunable nanoscale structures, 3D designs, and conductive properties. MP$\mu$SL advantageously offers control in customizing 3D objects and, in combination with novel polymer compositions, provides an exciting approach for designing and optimizing additive manufacturing technologies.

## ■ ASSOCIATED CONTENT

### Supporting Information

Materials and instrumentation, synthetic methods, MP$\mu$SL working curves, and related fabrication details. This material is available free of charge via the Internet at http://pubs.acs.org.

## ■ AUTHOR INFORMATION

### Corresponding Author

*E-mail: telong@vt.edu.

### Notes

The authors declare no competing financial interest.

## ■ ACKNOWLEDGMENTS

We acknowledge the Institute for Critical Technology and Applied Science (ICTAS) and the Design, Research, and Education for Additive Manufacturing Systems (DREAMS) laboratory at Virginia Tech for instrument support. We also thank Dr. Rolf Mueller in the Department of Mechanical Engineering for access to the microCT instrumentation.

## ■ REFERENCES

(1) Allen, M. H.; Hemp, S. T.; Zhang, M.; Zhang, M.; Smith, A. E.; Moore, R. B.; Long, T. E. *Polym. Chem.* **2013**, *4*, 2333.
(2) Lu, J.; Yan, F.; Texter, J. *Prog. Polym. Sci.* **2009**, *34*, 431.
(3) Obadia, M. M.; Mudraboyina, B. P.; Serghei, A.; Phan, T. N.; Gigmes, D.; Drockenmuller, E. *ACS Macro Lett.* **2014**, *3*, 658.
(4) Godeau, G.; Navailles, L.; Nallet, F.; Lin, X.; McIntosh, T. J.; Grinstaff, M. W. *Macromolecules* **2012**, *45*, 2509.
(5) Cheng, S.; Zhang, M.; Wu, T.; Hemp, S. T.; Mather, B. D.; Moore, R. B.; Long, T. E. *J. Polym. Sci., Part A: Polym. Chem.* **2012**, *50*, 166.
(6) Hemp, S. T.; Smith, A. E.; Bryson, J. M.; Allen, M. H.; Long, T. E. *Biomacromolecules* **2012**, *13*, 2439.
(7) Jangu, C.; Wang, J. H. H.; Wang, D.; Sharick, S.; Heflin, J. R.; Winey, K. I.; Colby, R. H.; Long, T. E. *Macromol. Chem. Phys.* **2014**, *215*, 1319−1331.
(8) Gao, R.; Wang, D.; Heflin, J. R.; Long, T. E. *J. Mater. Chem.* **2012**, *22*, 13473.
(9) Wu, T.; Wang, D.; Zhang, M.; Heflin, J. R.; Moore, R. B.; Long, T. E. *ACS Appl. Mater. Interfaces* **2012**, *4*, 6552.
(10) Freeman, B. D. *Macromolecules* **1999**, *32*, 375.
(11) Zhang, Y.; Zhang, S.; Lu, X.; Zhou, Q.; Fan, W.; Zhang, X. P. *Chem.—Eur. J.* **2009**, *15*, 3003.
(12) Lin, H.; Wagner, E. V.; Swinnea, J. S.; Freeman, B. D.; Pas, S. J.; Hill, A. J.; Kalakkunnath, S.; Kalika, D. S. *J. Membr. Sci.* **2006**, *276*, 145.
(13) Wang, S.-W.; Liu, W.; Colby, R. H. *Chem. Mater.* **2011**, *23*, 1862.
(14) Gu, S.; Cai, R.; Yan, Y. *Chem. Commun.* **2011**, *47*, 2856.
(15) Noonan, K. J. T.; Hugar, K. M.; Kostalik, H. A.; Lobkovsky, E. B.; Abruna, H. D.; Coates, G. W. *J. Am. Chem. Soc.* **2012**, *134*, 18161.
(16) Moore, C. M.; Hackman, S.; Brennan, T.; Minteer, S. D. *J. Membr. Sci.* **2005**, *254*, 63.
(17) Yan, X.; He, G.; Gu, S.; Wu, X.; Du, L.; Wang, Y. *Int. J. Hydrogen Energy* **2012**, *37*, 5216.
(18) Hemp, S. T.; Zhang, M.; Allen, M. H., Jr.; Cheng, S.; Moore, R. B.; Long, T. E. *Macromol. Chem. Phys.* **2013**, *214*, 2099.
(19) Chen, H.; Choi, J.-H.; Salas-de la Cruz, D.; Winey, K. I.; Elabd, Y. A. *Macromolecules* **2009**, *42*, 4809.
(20) Ohno, H.; Yoshizawa, M.; Ogihara, W. *Electrochim. Acta* **2004**, *50*, 255.
(21) Armand, M.; Endres, F.; MacFarlane, D. R.; Ohno, H.; Scrosati, B. *Nat. Mater.* **2009**, *8*, 621.
(22) Ghassemi, H.; Riley, D. J.; Curtis, M.; Bonaplata, E.; McGrath, J. E. *Appl. Organomet. Chem.* **1998**, *12*, 781.
(23) Hemp, S. T.; Zhang, M.; Tamami, M.; Long, T. E. *Polym. Chem.* **2013**, *4*, 3582.
(24) Borguet, Y. P.; Tsarevsky, N. V. *Polym. Chem.* **2012**, *3*, 2487.
(25) Wang, R.; Lowe, A. B. *J. Polym. Sci., Part A: Polym. Chem.* **2007**, *45*, 2468.
(26) Stokes, K. K.; Orlicki, J. A.; Beyer, F. L. *Polym. Chem.* **2011**, *2*, 80.
(27) Lambert, P. M.; Campaigne, E. A., III; Williams, C. B. Solid Freeform Fabrication Symposium, Austin, Texas, August 12−13, 2013, Univ. of Texas—Austin: Austin, Texas, 2013; p 111.
(28) Bertsch, A.; Lorenz, H.; Renaud, P. *Sens. Actuators A* **1999**, *73*, 14.
(29) Zheng, X.; Deotte, J.; Alonso, M. P.; Farquar, G. R.; Weisgraber, T. H.; Gemberling, S.; Lee, H.; Fang, N.; Spadaccini, C. M. *Rev. Sci. Instrum.* **2012**, *83*, 125001.
(30) Bertsch, A.; Zissi, S.; Jezequel, J.; Corbel, S.; Andre, J. *Microsyst. Technol.* **1997**, *3*, 42.
(31) Kuo, P.-L.; Wu, C.-A.; Lu, C.-Y.; Tsao, C.-H.; Hsu, C.-H.; Hou, S.-S. *ACS Appl. Mater. Interfaces* **2014**, *6*, 3156.
(32) Green, M. D.; Choi, J.-H.; Winey, K. I.; Long, T. E. *Macromolecules* **2012**, *45*, 4749.
(33) Bara, J. E.; Gabriel, C. J.; Lessmann, S.; Carlisle, T. K.; Finotello, A.; Gin, D. L.; Noble, R. D. *Ind. Eng. Chem. Res.* **2007**, *46*, 5380.
(34) Sanders, D. F.; Smith, Z. P.; Guo, R.; Robeson, L. M.; McGrath, J. E.; Paul, D. R.; Freeman, B. D. *Polymer* **2013**, *54*, 4729.
(35) Hatakeyama, E. S.; Ju, H.; Gabriel, C. J.; Lohr, J. L.; Bara, J. E.; Noble, R. D.; Freeman, B. D.; Gin, D. L. *J. Membr. Sci.* **2009**, *330*, 104.
(36) Sagle, A. C.; Ju, H.; Freeman, B. D.; Sharma, M. M. *Polymer* **2009**, *50*, 756.
(37) Lee, M.; Choi, U. H.; Colby, R. H.; Gibson, H. W. *Chem. Mater.* **2010**, *22*, 5814.
(38) Walker, C. N.; Versek, C.; Touminen, M.; Tew, G. N. *ACS Macro Lett.* **2012**, *1*, 737.